Microstructural and spectroscopic investigations into the effect of CeO_2 additions on the performance of a MnO_2 aqueous rechargeable battery

Manickam Minakshi [a,*], David R.G. Mitchell [b], Melody L. Carter [b], Dominique Appadoo [c], Kalaiselvi Nallathamby [d]

[a] *Faculty of Minerals and Energy, Department of Extractive Metallurgy, Murdoch University, Murdoch, WA 6150, Australia*
[b] *Materials and Engineering Science, ANSTO, PMB 1, Menai, NSW 2234, Australia*
[c] *Australian Synchrotron, Blackburn Road, Clayton, VIC 3168, Australia*
[d] *Central Electrochemical Research Institute, ECPS Division, Karaikudi, Tamilnadu 630006, India*

ARTICLE INFO

ABSTRACT

The influence of CeO_2 additions on the electrochemical behaviour of the MnO_2 cathode in a $Zn–MnO_2$ battery using lithium hydroxide (LiOH) as an electrolyte is investigated using microscopy and spectroscopic techniques. The results showed that such additions greatly improve the discharge capacity of the battery (from 155 to 190 mAh g^{-1}) but only from the second discharge cycle onwards. Capacity fade with subsequent cycling is also greatly reduced. With an aim to understand the role of CeO_2 on the discharge–charge characteristics of MnO_2 and its mechanism, we have used a range of microscopy, spectroscopy and diffraction-based techniques to study the process. The CeO_2 is not modified by multiple discharged and charged cycles. The CeO_2 may enhance the discharge–charge performance of the battery by raising the oxygen evolution potential during charging but does not take part directly in the redox reaction.

1. Introduction

Since its invention in 1865, the manganese dioxide (MnO_2) battery has continuously been improved starting with the earliest zinc–manganese dry battery, then $Zn–MnO_2$ primary battery and culminating with the current commercially available alkaline zinc–MnO_2 battery [1]. This battery type is still in high demand in the consumer market because it is mercury-free, provides high rate capability and the cost is significantly lower than for the dominant rechargeable lithium-ion battery [2,3]. The primary reasons for using MnO_2 as a cathode material are its low cost, low toxicity and high availability compared with competing battery materials such as Co and Ni [4]. Also, from a thermodynamical point of view, MnO_2 is the most stable form of tetravalent Mn [5] to retain oxygen at standard temperature and oxygen pressure, whereas Co and Ni are thermally unstable [6]. Therefore, MnO_2-based cathodes are attractive for energy storage applications ranging from alkaline to lithium batteries and even to supercapacitors [7,8].

In the $Zn–MnO_2$ battery, the good discharge performance of MnO_2 has motivated researchers to make these batteries rechargeable [9,10]. This would lead more sustainable use of available manganese resources. Among the various polymorphs of MnO_2 [11,12], γ-MnO_2 of the type IBA-32 (International Battery Association) is used in our aqueous $Zn–MnO_2$ system. Recently, we showed that lithium intercalation can occur in a $Zn–MnO_2$ battery using aqueous LiOH electrolytes [13]. Further to this, in an attempt to improve the overall performance of this aqueous rechargeable cell we have investigated various additives like TiS_2 [14], TiB_2 [15] and Bi_2O_3 [16] made to the MnO_2 cathode. These additives significantly improve the discharge performance of MnO_2 battery by stabilizing the MnO_2 crystal lattice. This enhances the amount of lithium intercalated into the host MnO_2 structure.

In this paper we report on cerium oxide (CeO_2) modified MnO_2 cathodes that offer an improved discharge capacity. Somewhat surprisingly, this improvement is only evident following the first charging cycle. Cerium oxide is one of the most reactive rare earth metal oxides, and is commonly used as a promoter or support in industrial catalytic processes due to its oxygen storage capacity [17–19]. Cerium oxide also has good electrical conductivity and diffusivity at ambient temperature [20]. To the best of our knowledge, there has been no work performed on CeO_2 additions to MnO_2 for battery applications. Very recently we carried out an

electrochemical characterization into the influence of variable levels of CeO_2 addition [21] and found increasing the additive level beyond 2 wt.% causes a decrease in cell capacity on long term cycling. Hence, in this paper, we have confined our results only to 2 wt.% addition. The objective of this work is (a) to understand the role of CeO_2 by comparing the electrochemical results with those of the previously published pure MnO_2 (no additive) [22] and (b) to examine the electrode reactions of the discharged–charged cathode using transmission electron microscopy (TEM), X-ray diffraction (XRD) and infra-red spectroscopy (IR).

2. Experimental

The electrolytic manganese dioxide (EMD; γ-MnO_2) type (IBA sample 32) material used in this work was purchased from the Kerr McGee Chemical Corporation. Cerium oxide (CeO_2) was obtained from Aldrich Chemical Company. For the electrochemical test, a pellet was prepared by mixing 73 wt.% MnO_2 consisting of 2 wt.% CeO_2 with 20 wt.% acetylene black (A-99, Asbury, USA) and 5 wt.% poly (vinylidene difluoride) (PVDF, Sigma–Aldrich) binder in a mortar and pestle. An electrochemical cell was constructed with the disk-like pellet as the cathode, Zn metal as the anode and filter paper as the separator. The electrolyte was a saturated solution of lithium hydroxide (LiOH) containing $1\,mol\,L^{-1}$ zinc sulphate ($ZnSO_4$) with a pH equivalent to 10.5. The cell design and its experimental details were similar to those reported earlier [13].

The morphology and interplanar spacings of the products formed before and after discharge were characterized by transmission electron microscopy (TEM), high-resolution TEM (HRTEM) and electron energy loss spectroscopy (EELS) using a JEOL 2010F TEM model operated at 200 kV. TEM specimens were prepared by grinding a small fragment scraped from the pressed pellet under methanol and dispersing on a holey carbon support film. Specimens were examined at liquid nitrogen temperature in a cooling stage, to reduce beam damage and contamination effects. For X-ray analysis a Siemens D500 X-ray diffractometer 5635 using Co Kα radiation was used. The voltage and current were 30 kV and 40 mA. The scan rate was 1°/min. Two theta values were recorded between 20° and 60°. For infrared (IR) analysis, powdered MnO_2 samples were mixed with potassium bromide (KBr) and pressed into disk shaped pellets. These pellets were then mounted on a sample holder and analyses were carried out under vacuum (for an improved performance in mid infrared absorbing H_2O and CO_2) on IFS 125 HR spectrometer (at Australian Synchrotron) using globar as the internal source with 4 mm of aperture in the mid infrared region between 650 and $1500\,cm^{-1}$. The IR absorption spectra were obtained by taking the ratio of the sample spectra to a background (KBr) spectra. The data acquisition was made on OPUS NT software.

3. Results and discussion

The multiple galvanostatic discharge–charge curves of 2 wt.% cerium oxide/MnO_2 cathode with zinc as anode are shown in Fig. 1. The cell was discharged and charged at a constant current density of $0.5\,mA\,cm^{-2}$ with lower and upper cut-off voltages of 1.0 and 1.9, respectively. The first discharge capacity of the CeO_2 modified cell was $155\,mAh\,g^{-1}$ while $148\,mAh\,g^{-1}$ [14] was obtained from the unmodified cell (no additives). This shows that the effect of cerium oxide on the first discharge cycle is negligible. However, on the second discharge cycle of the CeO_2 modified cell, the utilization of the material was 18% higher with the capacity increased to $190\,mAh\,g^{-1}$. After multiple discharge cycles (5th cycle) the discharge capacity of this cell was still higher ($183\,mAh\,g^{-1}$) than the unmodified cell. Fig. 2 compares the cyclabilities of the CeO_2 modified and unmodified cell. The CeO_2 addition improved the cell discharge capacity but only from the second cycle. The role of
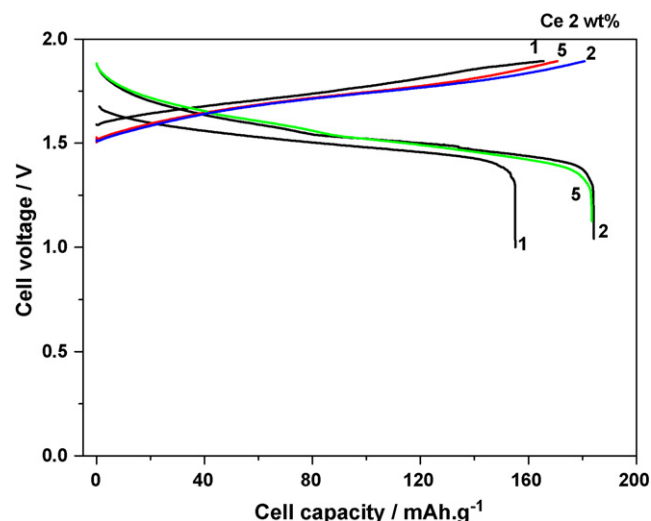
Fig. 1. Discharge–charge profiles of CeO_2 modified MnO_2 cathode with Zinc as an anode. Cycle numbers are indicated in the figure. The striking behaviour here is the difference observed from the 1st and subsequent cycle.

cerium oxide as an additive was initially unclear because if it takes part in the reduction/oxidation processes then the first discharge capacity should be higher but that is not observed in Figs. 1 and 2. Hence, in order to elucidate the role of CeO_2 the nature of the cathode material before and after discharge and charge was characterized.

The TEM image of the CeO_2 modified MnO_2 before discharge is shown in Fig. 3. The bright field image showed the MnO_2 to be crystalline and defective. The selected area diffraction (SADP) on this area (Fig. 3a inset) showed the lowest index MnO_2 reflections to be quite diffuse, supporting this. The measured d-spacings were in good agreement with those reported for MnO_2 ramsdellite structure [23]. Fig. 3b shows a region of MnO_2 containing CeO_2 particles. These were distinct from the MnO_2 particles in that they were more angular (Fig. 3b) and showed very strong diffraction and kikuchi line contrast, due to the higher mean atomic number and less defective crystal structure, respectively. Selected area diffraction of the CeO_2 particles (not shown) yielded spacings consistent with the CeO_2 phase [24]. The CeO_2 particles were typically quite coarse being 100–500 nm in diameter. Electron energy loss
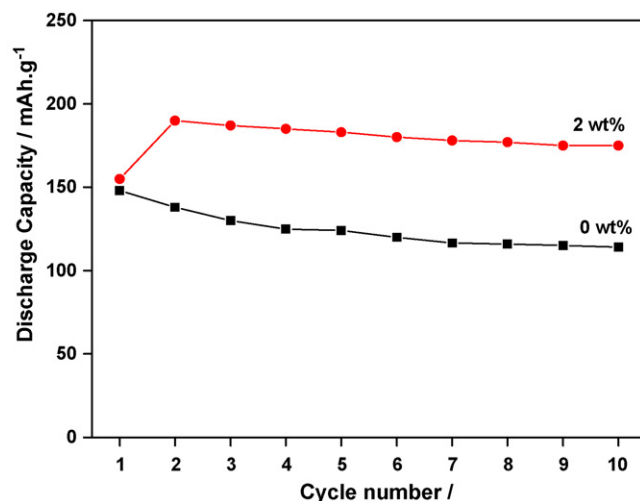
Fig. 2. Variation of discharge capacity as a function of cycle number for the CeO_2 modified MnO_2 and un-modified MnO_2 cell. Amount of CeO_2 additions are indicated in the figure.
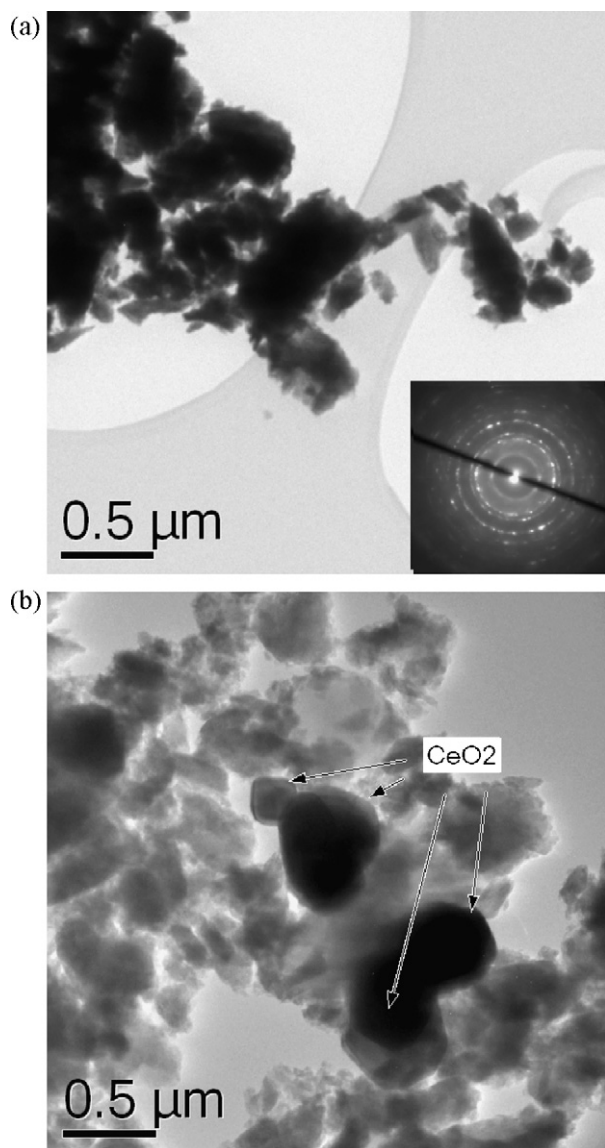
Fig. 3. TEM image of the CeO$_2$ modified MnO$_2$ before discharge (a) bright field image of MnO$_2$ particles – inset shows its corresponding selected area diffraction (SADP) and (b) bright field image of CeO$_2$ particles.

Fig. 4. EELS Ce M$_{4,5}$ spectrum for CeO$_2$ modified MnO$_2$ (a) before and (b) after discharge.

spectroscopy of the MnO$_2$ phase yielded a mean branching ratio of 0.678 ± 0.005 suggesting the valence state of the Mn in MnO$_2$ is +4 [14]. The CeO$_2$ particles produced consistent EELS spectra, an example of which is shown in Fig. 4a. The CeO$_2$ EELS spectra showed an intense M$_{4,5}$ doublet at around 900 eV. Each of these peaks is further split into a high-energy shoulder. The spectra obtained here are very similar to that reported for CeO$_2$ in the EELS Atlas for CeO$_2$ [25]. Bright field imaging (Fig. 5a) of the CeO$_2$ modified material after the first discharge cycle showed the presence of spherical carbon (from acetylene black) and angular MnO$_2$ particles. Some organic regions were rich in fluorine from the PVDF as binder. Phase identification was confirmed with X-ray microanalysis – not shown. The corresponding diffraction pattern (Fig. 5a inset) shows streaking indicating lamellar structures with short-range order. The dark field image of the MnO$_2$ shows the lamellar structure (Fig. 5b) which could be related to MnOOH phase [26]. Bright field imaging (Fig. 5c) showed angular CeO$_2$ particles were still present and appeared unchanged after the discharge cycle. The particles were 100–500 nm in diameter and were single crystal. Selected area diffraction of the CeO$_2$ confirmed it was unchanged by

the discharge cycle. The EELS analysis of the discharged CeO$_2$ modified sample also suggested that the CeO$_2$ particles were unchanged by the discharge process. The characteristic edge shape (Fig. 4b) was identical to that found in the material prior to discharge (Fig. 4a).

The CeO$_2$ modified MnO$_2$ particles after the first charge cycle were similar to those in the discharged state (Fig. 5a). Some elongated Zn- and O-rich crystals were found (X in Fig. 6a). The MnO$_2$ was highly defective (Fig. 6b) and selected area diffraction (not shown) yielded spacings consistent with MnO$_2$. As before, streaking was present. Bright field imaging of the CeO$_2$ particles (Fig. 7a) showed them to be highly crystalline. Selected area diffraction (Fig. 7b inset) highlighted the differences between the patterns for the two phases. The MnO$_2$ was poorly crystalline and contained disorder, resulting in diffuse diffraction features. The CeO$_2$ was highly crystalline and defect-free resulting in very sharp diffraction rings. The CeO$_2$ EELS spectrum (not shown) was identical to those shown in Fig. 4a and b (before and after discharge, respectively) showing the CeO$_2$ to be unchanged by the electrochemical cycling. Even after many cycles, EELS spectra for the CeO$_2$, were identical to those of discharged and charged samples, showing that the CeO$_2$ was not modified by the electrochemical cycling. Although the CeO$_2$ was unchanged an increase in the first charge capacity of 18% was observed and this increased capacity was retained on subsequent cycling. It is widely know that CeO$_2$ is an excellent material to release and absorb oxygen reversibly during redox reactions [27]. Hence, this suggests that the cerium oxide may increase the oxygen evolution potential during charging. Oxygen evolution is an unwanted reaction which normally occurs on the positive electrode during charging in the aqueous electrolyte. Suppression of this reaction may therefore encourage more complete conversion of the LiMnO$_2$ phase back to MnO$_2$ during charging. The effect of CeO$_2$ was only evident after the first charge cycle, with no influence found during the first discharge cycle. Capacity fading was evident with the pure MnO$_2$ cathode, but not in the case of the CeO$_2$ modified material. This suggests that in pure MnO$_2$ (no additive), a portion of charging process is consumed by oxygen evolution and upon cycling some of the MnO$_2$ cathode transforms into less electro-active forms, like manganese oxyhydroxides, limiting the discharge capacity [22]. Capacity fading was not a feature of the CeO$_2$ modified material. In part this may be due to CeO$_2$ helping to stabilize the MnO$_2$ lattice in a manner similar to that described for other additives such as TiS$_2$, TiB$_2$ and Bi$_2$O$_3$. In addition, the suppression of oxygen evolution reactions may also provide a stronger thermodynamic driving force to transform any of the less electro-active phases which do form, back to the desired MnO$_2$ phase.

Fig. 8a–c show X-ray diffraction patterns of the CeO$_2$ modified cathode before and after discharge, and after charging, respectively.
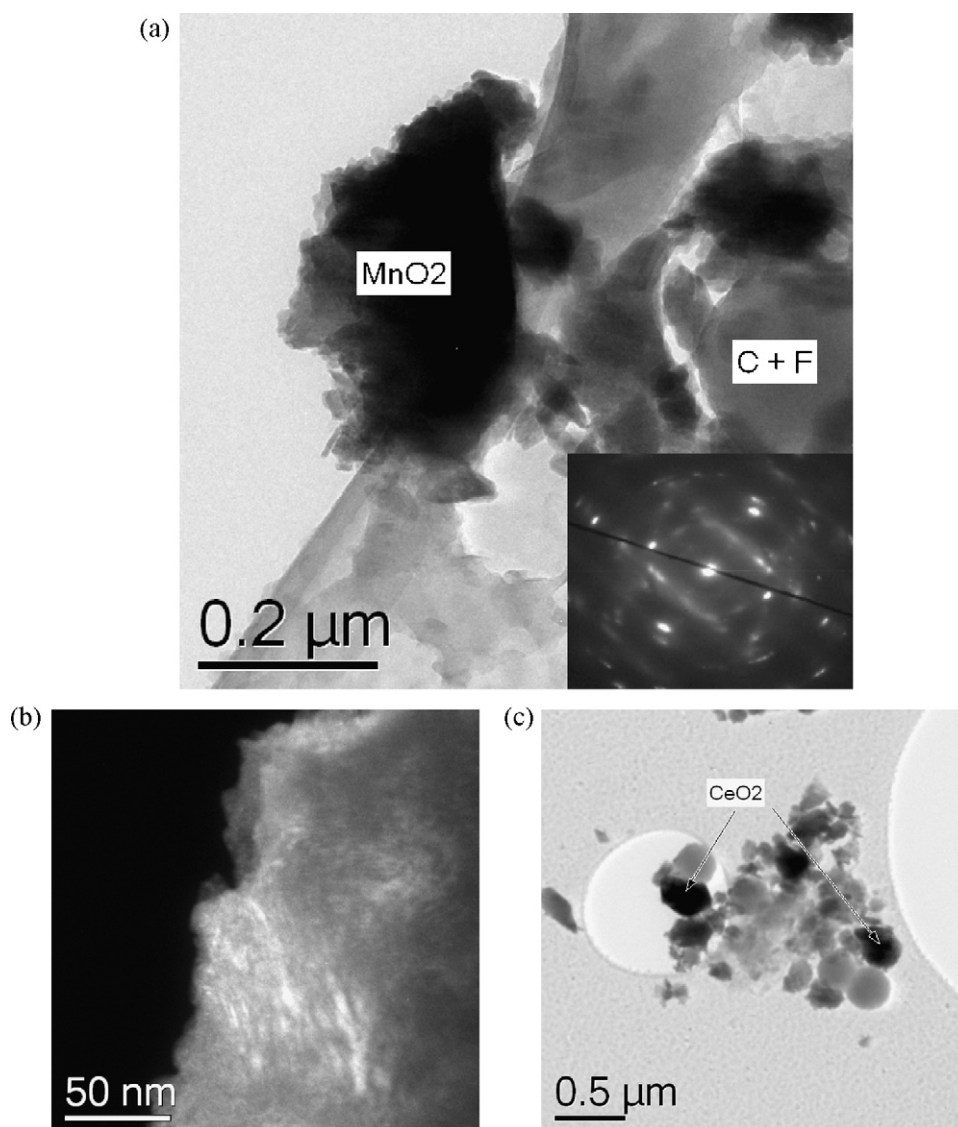
Fig. 5. TEM image of the CeO$_2$ modified MnO$_2$ after discharge (a) bright field image of MnO$_2$ particles – inset shows its corresponding selected area diffraction (SADP), (b) dark image of the formation of lamellar structure and (c) bright field image of CeO$_2$ particles.

The before discharge material (Fig. 8a) shows the characteristic peaks of MnO$_2$ and CeO$_2$ as quoted in the JCPDS database [23,24]. The discharged cathode (Fig. 8b) shows the emergence of new peaks (*, ◯, □ and ●). The main Bragg reflection corresponding to graphite (acetylene black) is seen at $2\theta = 30°$ (C). The original peaks of MnO$_2$ (+) are replaced by those of a number of new phases whereas the peaks corresponding to CeO$_2$ are almost unchanged. As indexed in the XRD pattern these new reflections are in good agreement with
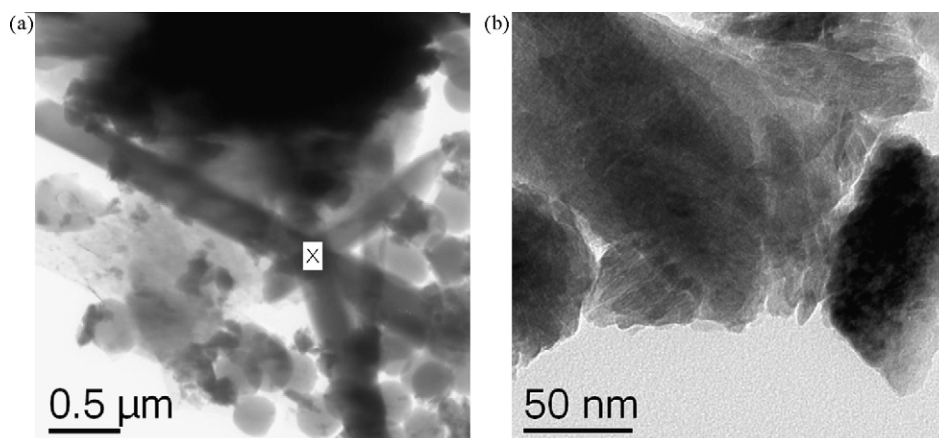
Fig. 6. TEM image of the CeO$_2$ modified MnO$_2$ after charge (a) bright field image showing Zn- and O-rich crystals (at X) and (b) defective MnO$_2$.

(a)

(b)
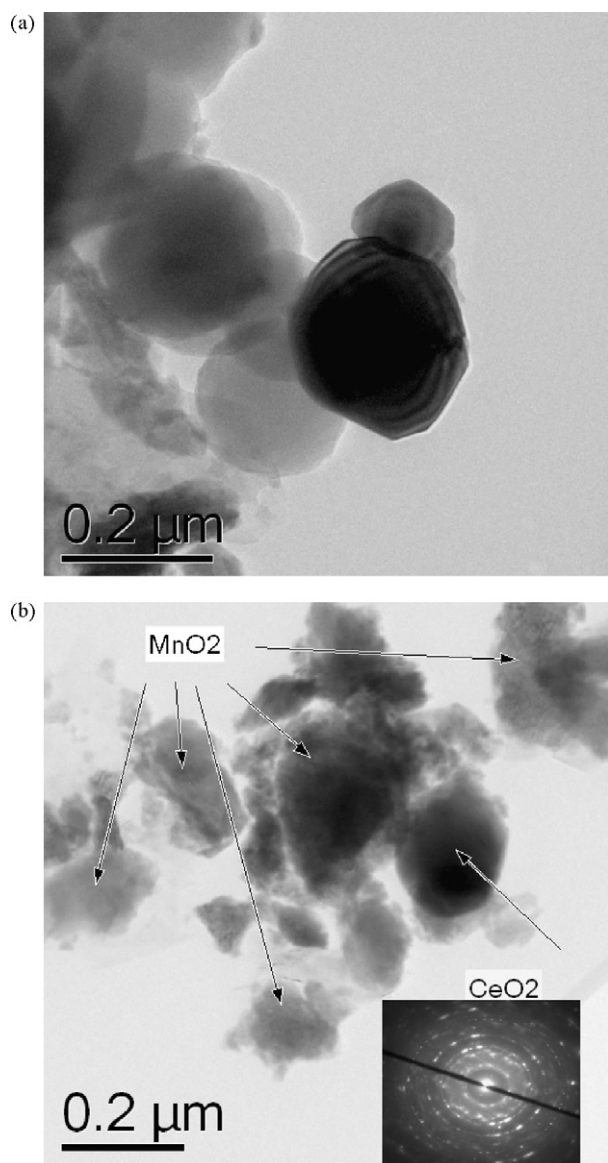
Fig. 7. TEM images of the CeO_2 modified MnO_2 after charge. Bright field images of (a) region rich in CeO_2 particles and (b) region containing MnO_2 and CeO_2 particles – inset showing its selected area diffraction (SADP).

those reported for the following materials: Mn_2O_3 (*), MnOOH ($\bigcirc$), MnO ($\square$) and Li_xMnO_2 ($\bullet$), i.e. lithium intercalated MnO_2 [23,24,28]. This shows that during discharge manganese is, in part, reduced to various oxyhydroxides and lithium is also intercalated into the MnO_2 structure to form Li_xMnO_2. The XRD pattern for the charged cathode material (Fig. 8c) was also similar to that of the starting material except a few minor reflections were present identified as being due to Mn_2O_3 and Li_xMnO_2. The CeO_2 peaks were very similar suggesting that ceria is not modified in the electrochemical process. However, peaks corresponding to manganese oxides and hydroxides and lithium intercalated MnO_2 disappear on charging indicating that the electrochemical process is reversible in the presence of CeO_2.

Infrared spectroscopy has been used to provide further insight into the influence of CeO_2 modified MnO_2 cathode. It is reported that fundamental vibrations of MnO_2 are generated in the far infrared region while those at mid infrared are due to hydrous components of the manganese oxides [29]. The region of interest in this work is the mid infrared, for the samples before and after discharge.
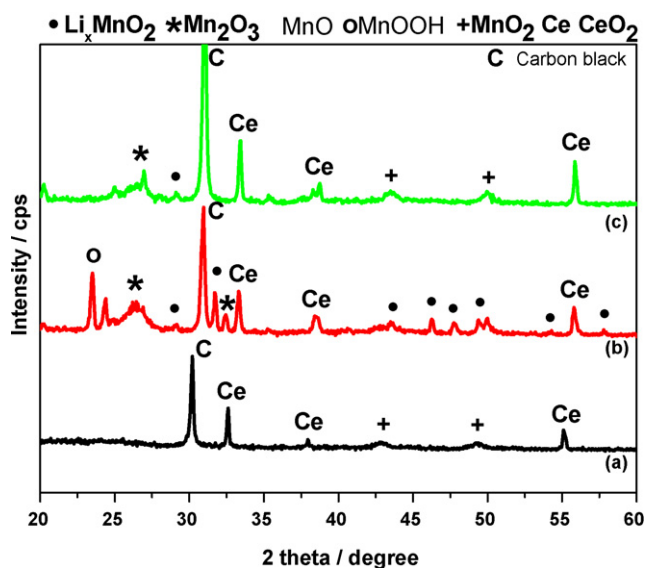
Fig. 8. XRD patterns of CeO_2 modified MnO_2 (a) before discharge, (b) discharged and (c) charged samples.
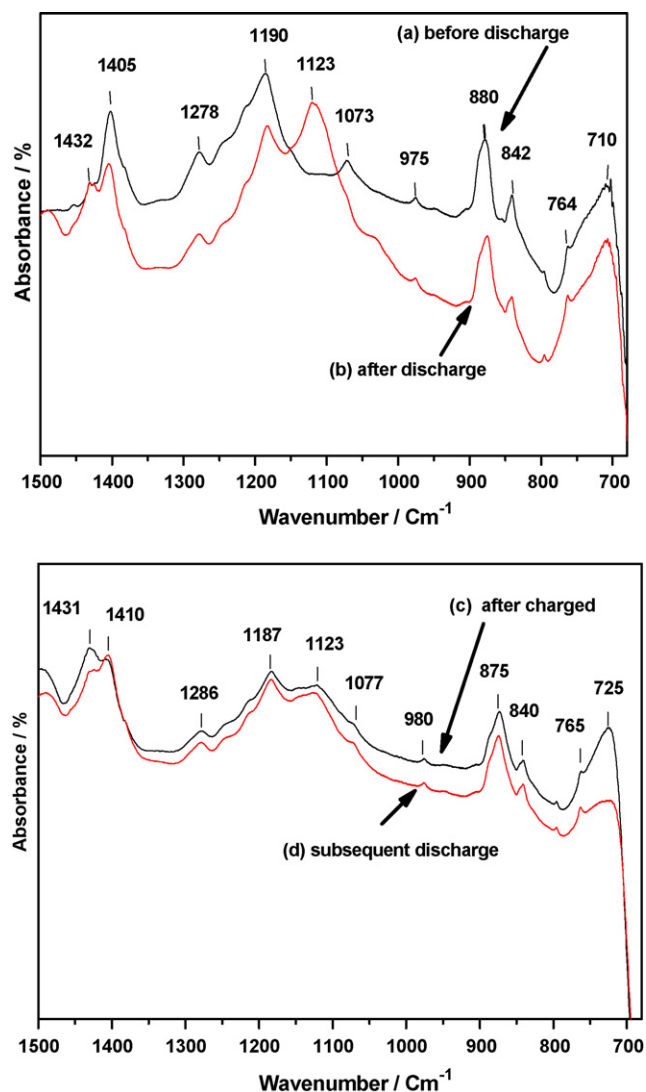
Fig. 9. Mid infrared spectra of CeO_2 modified MnO_2 (a) before discharge, (b) discharged (c) charged and (d) subsequent discharged samples.

These are compared in Fig. 9a and b. For the discharged sample, new absorption peaks at 1123 and 1432 cm^{-1} are seen. The strong peak at 1123 cm^{-1} demonstrates the existence of γ-OH bonding [30] and the broad peak around 2600 cm^{-1} region (not shown here) is the OH stretching related to the hydrogen bonding [29–31] corresponding to the MnOOH structure. This confirms the behaviour observed through TEM and XRD analysis, namely that manganese oxyhydroxides are formed during discharge. A small vibrational peak at 1432 cm^{-1} in the discharged sample could be related to manganese (II) oxides [29]. The mid infrared spectra of the second charge (Fig. 9c) and second discharge cycle (Fig. 9d) were very similar. In contrast to Fig. 9a and b, the absorption peaks at 1123 and 1432 cm^{-1} region were much lower in. These results indicate that manganese oxyhydroxides and oxides are formed only during the first discharge cycle. These unwanted products are shown to be suppressed during charging and further discharging in the presence of CeO_2. This addition clearly enhances the discharge capacity during subsequent cycling.

4. Conclusions

The electrochemical performance of CeO_2 modified MnO_2 cathode in an aqueous rechargeable battery has been investigated using microscopy and spectroscopic techniques. The CeO_2 additive enhanced the performance of the battery, increasing the capacity from 155 to 190 mAh g^{-1} on the second discharge cycle, representing an increase of 18%. Importantly, this increased capacity was retained on subsequent cycling. As reported in our earlier work, when using pure MnO_2 (no additive) the corresponding cell exhibited a constant capacity fading on subsequent cycling. The influence of CeO_2 may in part arise from a stabilizing effect on the MnO_2 crystal lattice during discharge, such as has been found for compounds such as TiB_2 and Bi_2O_3. The CeO_2 may also increase the oxygen evolution potential on the MnO_2 cathode during charging. This results in a greater thermodynamic driving force to transform both lithium intercalated MnO_2 (Li_xMnO_2) along with any less electroactive oxides/hydroxides of Mn back into MnO_2 during charging, thus suppressing the capacity loss.

References

[1] R.K. Ghavami, Z. Rafiei, S.M. Tabatabaei, J. Power Sources 164 (2007) 934.
[2] C.-C. Yang, S.-J. Lin, J. Power Sources 112 (2002) 174.
[3] C.M. Julien, Mater. Sci. Eng. R 40 (2003) 47.
[4] N.N. Greenwood, A. Earnshaw, Chemistry of the Elements, first ed., Pergamon Press, Oxford, 1984, p. 1212.
[5] S. Fritsch, A. Navrotsky, J. Am. Ceram. Soc. 79 (1996) 1761.
[6] D.D. MacNeil, Z. Lu, Z. Chen, J.R. Dahn, J. Power Sources 108 (2002) 8.
[7] Y. Kuzoka, C.J. Wen, J. Otomo, M. Ogura, T. Kobayashi, K. Yamada, H. Takahashi, Solid State Ionics 175 (2004) 507.
[8] S.F. Chin, S.C. Pang, M.A. Anderson, J. Electrochem. Soc. 149 (2002) A379.
[9] Y. Shen, K. Kordesch, J. Power Sources 87 (2000) 162.
[10] Y. Sharma, M. Aziz, J. Yusof, K. Kordesch, J. Power Sources 94 (2001) 129.
[11] M.M. Thackeray, Prog. Solid State Chem. 25 (1997) 1.
[12] S. Chou, F. Cheng, J. Chen, J. Power Sources 162 (2006) 727.
[13] M. Minakshi, P. Singh, T.B. Issa, S. Thurgate, R. DeMarco, J. Power Sources 130 (2004) 254.
[14] M. Minakshi, D.R.G. Mitchell, P. Singh, Electrochim. Acta 52 (2007) 3294.
[15] M. Minakshi, D.R.G. Mitchell, K. Prince, Solid State Ionics 179 (2008) 355.
[16] M. Minakshi, D.R.G. Mitchell, Electrochim. Acta 53 (2008) 6323.
[17] C. Tang, Y. Bando, B. Liu, D. Golberg, Adv. Mater. 17 (2005) 3005.
[18] G.M. Christie, F.P.F. van Berkel, Solid State Ionics 83 (1996) 17.
[19] R. Si, Y.-W. Zhang, S.-J. Li, B.-X. Lin, C.-H. Yan, J. Phys. Chem. B 108 (2004) 12481.
[20] J. Bai, Z. Xu, Y. Zheng, H. Yin, Mater. Lett. 60 (2006) 1287.
[21] M. Minakshi, N. Kalaiselvi, D.R.G. Mitchell, J. Alloys and Compounds (2009) doi:10.1016/j.jallcom.2008.12.143.
[22] M. Minakshi, P. Singh, D.R.G. Mitchell, J. Electrochem. Soc. 154 (2007) A109.
[23] JCPDS Card (No. 43-1455).
[24] JCPDS Card (No. 34-0394).
[25] C.C. Ahn, O.L. Krivanek, EELS Atlas, Gatan Inc., 780 Commonwealth Drive, Warrendale, Pennsylvania, 1983, p. 15086.
[26] Y. Zhang, Y. Liu, F. Guo, Y. Hu, X. Liu, Y. Qian, Solid State Commun. 134 (2005) 523.
[27] Lj. Kudakovic, M. Flytzani-Stephanopoulos, J. Catal. 179 (1998) 203.
[28] JCPDS Card (No. 44-0143).
[29] R.M. Potter, G.R. Rossman, Am. Mineral. 64 (1979) 1199.
[30] Y.-T. Wu, C.-C. Hu, Electrochem. Solid State Lett. 8 (2005) A240.
[31] A. Novak, Struct. Bond 18 (1974) 177.